Journal of Power Sources 396 (2018) 774–781

Contents lists available at ScienceDirect

Journal of Power Sources

journal homepage: www.elsevier.com/locate/jpowsour

Extreme fast charging characteristics of zirconia modified $LiNi_{0.5}Mn_{1.5}O_4$ cathode for lithium ion batteries

Umair Nisar[a,c], Ruhul Amin[b,**], Rachid Essehli[b], R.A. Shakoor[a], Ramazan Kahraman[d], Do Kyung Kim[c], Mohammad A. Khaleel[f], Ilias Belharouak[e,*]

[a] Center for Advanced Materials (CAM), Qatar University, Doha, Qatar
[b] Qatar Environment and Energy Research Institute, Hamad Bin Khalifa University, Qatar Foundation, Doha, Qatar
[c] Department of Materials Science and Engineering, Korea Advanced Institute of Science and Technology (KAIST), Republic of Korea
[d] Department of Chemical Engineering, College of Engineering, Qatar University, Doha, Qatar
[e] Energy and Transportation Science Division, Oak Ridge National Laboratory, Oak Ridge, TN, USA
[f] Energy and Environmental Sciences Directorate, Oak Ridge National Laboratory, Oak Ridge, TN, USA

HIGHLIGHTS

- ZrO_2-$LiNi_{0.5}Mn_{1.5}O_4$ withstands 80C-rate and demonstrates over thousand cycles at 40C.
- Charge transfer resistance at $LiNi_{0.5}Mn_{1.5}O_4$/electrolyte is stable with coating.
- Origin of high-rate capability is correlated with the high kinetics at the material's interfaces.
- Surface modification of $LiNi_{0.5}Mn_{1.5}O_4$ enables extreme fast charging.

GRAPHICAL ABSTRACT

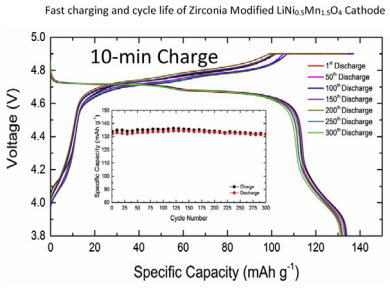

ARTICLE INFO

Keywords:
Extreme fast charging
$LiNi_{0.5}Mn_{1.5}O_4$
Spinel
Electric vehicles
Lithium ion batteries
Zirconia coating

ABSTRACT

$LiNi_{0.5}Mn_{1.5}O_4$ is a promising high-voltage cathode for lithium-ion battery fast charging applications. Aware of its electrochemical stability issues, the material's surface is modified with small amounts of zirconia (ZrO_2) ranging from 0.5 to 2 wt% using a scalable ball milling process. The advantage of the coating has been demonstrated in electrochemical measurements performed at room temperature and 55 °C, and in cells discharged under high-rate conditions up to 80C. Of significance, the material coated with 1.0 wt% ZrO_2 has been cycled at the 40C rate for over a thousand cycles and retains 86% of its initial capacity. The material with 2.0 wt% ZrO_2 modification preserves 76% of its initial capacity when cycled at the 40C rate and 55 °C. The coated materials have shown excellent cycling stability when subjected to 6C (10-min) fast charging and C/3 discharging for 300 cycles. Compared to the uncoated material, the interfacial resistance of the zirconia modified $LiNi_{0.5}Mn_{1.5}O_4$ has been found to be much lower and does not significantly increase with increasing the coating amount. However, the electrochemical performances are still partly limited by both interfacial resistance at the beginning of charge and electrolyte diffusivity, particularly under higher rate cycling conditions. Overall, the strategy of ZrO_2 surface modification applied to $LiNi_{0.5}Mn_{1.5}O_4$ unveils the potential that the material could play in extreme fast charged electric vehicles.

* Corresponding author.
** Corresponding author.
E-mail addresses: mdruhul@hbku.edu.qa (R. Amin), khaleelma@ornl.gov (M.A. Khaleel), belharouaki@ornl.gov (I. Belharouak).

https://doi.org/10.1016/j.jpowsour.2018.06.065
Received 8 April 2018; Received in revised form 23 May 2018; Accepted 15 June 2018

1. Introduction

The fast-growing markets for consumer electronics, electric vehicles and renewable energies are increasingly catalyzing the development of advanced battery systems that are suitable in terms of energy and power densities, safety, cost and performance for the various energy applications [1,2]. Due to high-voltage and -energy density advantages, lithium-ion batteries have dominated the portable electronics market since last two decades, and are making steady strides towards the electrification of personal and public transportation [3–5]. Currently, lithium ion batteries have completely captured the portable electronics market, and the goal is now directed towards more penetration in electric vehicles (EVs) [3,6,7]. Yet, the available Li-ion battery technology still suffer from safety and energy density weaknesses, and in particular, from the fast charging shortcoming that may not catalyze the wide acceptance of electric vehicles.

At the materials level, the spinel $LiNi_{0.5}Mn_{1.5}O_4$ (labeled LNMO) is a very promising cathode due to its high energy density resulting from the product of its high-operating voltage (4.7 V vs. Li) and theoretical capacity (147 $mAh.g^{-1}$). However, the unsatisfactory cycling performance must be addressed prior to enabling the material in commercial lithium-ion batteries. Indeed, the coupling of the oxidation of electrolytes and parasitic reactions during the high-voltage operation of $LiNi_{0.5}Mn_{1.5}O_4$ leads to rapid capacity fade, especially at elevated temperature where manganese dissolution further degrades the cycle life [8–12]. Recently published review reports discussed details regarding the merit and major shortcomings of the material [13,14]. To mitigate these issues, several research approaches had been adopted including the doping for Mn/Ni [15–20], particles size and morphology tailoring [21–24], structural disorder and lithium concentration tuning [25,26], and surface modification [27–30]. The latter involved the use of various coating materials such as Al_2O_3, SiO_2, ZrO_2, TiO_2, MgO, and ZnO in order to reduce the undesirable interfacial side reactions, and hence improve the cycle life of LNMO [27,30–34]. Recently published reports on ZrO_2 as a coating material showed good performance of this material [35,36]. The caveat is that most of these surface modification approaches used complex chemical processes with difficulties in controlling the uniformity and thickness of these coatings [37–39]. In many instances, the interfacial resistance, which originates from the coating, can rather hinder the rate capability of the material.

Instead, any reliable coating approach on battery materials should be first cost effective and scalable despite any performance improvements. Second, there are still substantial uncertainties on how these coatings work in enhancing the electrochemical performance [25,28–32]. Indeed, it appears that nano-sized thin coatings can help in providing some improvements in battery cycle and calendar lives; however, thick coatings may act as a migration barrier for lithium transport resulting in capacity and rate performance decays [37,40]. Consequently, a quantitative study is needed to unveil the trade-off between the interfacial transport/kinetics (capacity and rate capability) and interfacial protection (cycle life) in a given battery coating strategy.

In this study, $LiNi_{0.5}Mn_{1.5}O_4$ has been coated with zirconia (ZrO_2) nano-size particles. Unlike most coating processes, the method involved the use of a soft and scalable ball milling technique in which increasing amounts of ZrO_2 (0.5–2 wt%) were introduced to $LiNi_{0.5}Mn_{1.5}O_4$ just before the final calcination. The obtained materials have been characterized by x-ray diffraction (XRD), scanning and transmission electron microscopies (SEM and TEM), and electrochemical charge and discharge. We also used the electrochemical impedance spectroscopy (EIS) to characterize the electrode/electrolyte interfaces before and after coatings. This process has resulted in significantly improving the life of $LiNi_{0.5}Mn_{1.5}O_4$ under high-temperature (55 °C) and high-rate performance (10-min charge) conditions. Our observation is that the material with 1.0 wt% ZrO_2 coating exhibited better rate performance at ambient temperature, while that with 2.0 wt% ZrO_2 coating showed better life span at 55 °C. The overall results demonstrated that the adopted ZrO_2-coating method could pave the way in enabling $LiNi_{0.5}Mn_{1.5}O_4$ as an advanced cathode material for extreme fast charging and long-cycle life lithium-ion battery applications.

2. Experimental

2.1. Materials preparation

$LiNi_{0.5}Mn_{1.5}O_4$ (LNMO) was prepared via sol-gel using lithium, nickel and manganese acetates (Sigma Aldrich) in the molar ratio 1.05:0.5:1.5, respectively. The precursors were dissolved in distilled water in the presence of citric acid. The molar ratio total-ions/citric-acid was 2:1. Ammonia was added to the transition metals solution dropwise until the pH of the solution reached 8. The resulting solution was kept at 70 °C until a transparent gel was obtained. The gel was dried in an oven at 100 °C, and then decomposed at 450 °C for 6 h in air before final calcination at 900 °C for 12 h. The surface modified LNMO was synthesized by addition of ZrO_2 nano-powder (Sigma Aldrich, < 100 nm (TEM)) to the material that was treated at 450 °C, and ball milling for 24 h using zirconia balls media. In this case, the nominal weight percentages of ZrO_2 in the composite were 0.5, 1.0, 1.5, 2.0 wt%. After ball milling, the composites ZrO_2-LNMO were calcined at 900 °C for 12 h in air. The heating and cooling rates were set at 5 °C/min.

2.2. Physical characterization

Powder-XRD (Rigaku) using Cu-Kα radiations was used to identify the phase purity of the synthesized materials. The particle morphology was investigated by field-emission scanning electron microscopy (FE-SEM, Hitachi S-4800). The material surface was investigated with X-ray photoelectron spectroscopy (XPS) (Thermo-Scientific-Sigma Probe).

2.3. Electrode fabrication

The positive electrodes were fabricated by casting slurries composed of 75 wt% LNMO active material or ZrO_2-LNMO, 17 wt% conductive carbon (Super-P) and 8 wt% poly (vinylidene fluoride) binder in 1-methyl-2-pyrrolidone (NMP) on an aluminum foil using doctor blade. The electrodes were dried at 80 °C to remove NMP, and then vacuum-dried at 120 °C to remove traces of moisture. The electrodes were cut into several disks of 12 mm diameter and 25 μm thickness. The active material loading was ~1 mg/cm^2 for all the measured cells.

2.4. Electrochemical measurements

Electrochemical measurements were carried out using 2032-type coin cells assembled with bare-LNMO or ZrO_2-LNMO in an Ar-filled glove box. Lithium foil was used as the negative electrode. The electrolyte was made of 1 M $LiPF_6$ dissolved in a solvent mixture of ethylene carbonate (EC) and dimethyl carbonate (DMC) (1:1 by v/v.). Galvanostatic charge/discharge tests were performed at 25 and 55 °C using Solartron battery cyclers (1470 E). The cells were tested under fast-charge and slow-discharge rate conditions and vice-versa to check the rate performance of the materials. To ensure reproducibility of results, several cells were subjected to the same testing conditions.

2.5. GITT and EIS measurements

The cells were initially charged and discharged using a current density equivalent to the C/10 rate to form stable solid electrolyte interphases (SEI) at both the positive and negative electrode interfaces. During a typical experiment, the C/10-equivalent current was applied at the start of the charge for 1 h to reach a certain state of charge, and then a 3-h rest was applied to reach the steady-state cell voltage. This procedure was repeated stepwise to cover all states of charge and

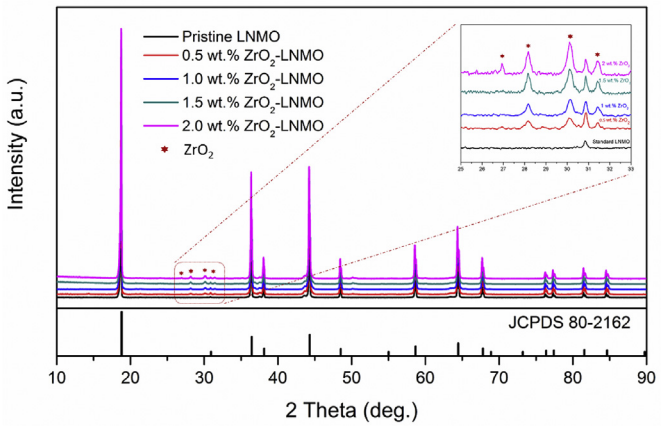

Fig. 1. XRD patterns of $LiNi_{0.5}Mn_{1.5}O_4$ and ZrO_2-modified LNMO (ZrO_2 content within 0.5–2.0 wt%).

discharge.

After partial delithiation/lithiation, the cells were kept at open circuit voltage (OCV) conditions to depolarize the cells, and then, to reach the steady state where the voltage decay was less than 1 mV/h at the end of the time interval. Thereafter, electrochemical impedance spectroscopy (EIS) measurements were performed in the frequency range of 2 MHz–5 mHz using a sinusoidal voltage amplitude of 10 mV. The obtained EIS spectra were fitted using an equivalent circuit model built in the ZView software. Numerical values were extracted from the EIS data using a complex non-linear least-squares regression analysis. The individual resistances of different electrochemical processes were extracted from the complex spectra.

3. Results and discussion

Fig. 1 shows the XRD patterns for the as-synthesized bare- and ZrO_2-modified $LiNi_{0.5}Mn_{1.5}O_4$. Both materials can be indexed according to $Fd\bar{3}m$ space group (JCPDS #80–2162) which is consistent with the formation of the spinel disordered phase ($LiNi_{0.5}Mn_{1.5}O_{4-\delta}$). This was expected since both materials were synthesized at 900 °C without further annealing at the phase transition temperature (650–700 °C) [41,42]. Oxygen deficiency ($\delta > 0$) is the reason behind the transition metal cationic disordered in the spinel phase as no NiO-based impurity was detected in the XRD patterns. In the case of the zirconia-modified sample, small peaks of crystalline ZrO_2 were observed between 25 and 32°. With increasing its amount, the intensity of the x-ray peaks of ZrO_2 also increased, as expected. We also noticed that the degree of disordered lies between 6 and 8% in the spinel structure as indicated by the voltage plateau observed at 4.0 V. Further details could be found in the electrochemical characterization part below.

Fig. 2 shows the SEM images of the as-prepared LNMO and ZrO_2-modified samples. The as-synthesized LNMO exhibited particle sizes in the range of 1.5–2 μm (Fig. 2a). With the addition of ZrO_2, the particle size slightly decreased to around 1 μm as shown in Fig. 2b–e. In comparison with the bare LNMO, the addition of ZrO_2 has resulted in a slight reduction of the particle size and in a relatively more homogeneous particle size distribution. Fig. 2f shows a typical TEM micrograph of the 2.0 wt% ZrO_2-modified LNMO in which we observed that the surface particle has been coated with ZrO_2 and that no zirconia agglomerations was present.

Fig. 3 shows the XPS spectra of the ZrO_2-modified $LiNi_{0.5}Mn_{1.5}O_4$ samples. The XPS analysis confirms the presence of ZrO_2 on the surface of LNMO. With increasing the amount of ZrO_2, the XPS peaks of the Zr^{4+} cation increased in intensity as illustrated in Fig. 3a–d. This result suggests that ZrO_2 was mainly distributed on the particles surface to form a relatively homogenous coating on LNMO. The binding energy of two separate peaks, as shown in Fig. 3, slightly shifted towards lower energies for the higher ZrO_2 percentages. This might be due to a relatively stronger interaction between the coating material and LNMO.

Fig. 4a shows the charge/discharge profiles of the cells comprising the bare- and ZrO_2-modified LNMO samples (0-2 wt% ZrO_2). The cells were charged and discharged at the 1C rate and exhibited the high (4.7 V) and low (4 V) voltage plateaus that are expected for the disordered spinel $LiNi_{0.5}Mn_{1.5}O_{4-\delta}$. An estimation of the degree of disorder was obtained by measuring the extent of the voltage plateau at 4.0 V which indicates the presence of 6–8% Mn^{3+} in the pristine sample. This plateau is caused by the activation of the redox couple Mn^{3+}/Mn^{4+}. Note that this is an extrinsic property of the spinel material which can vary depending upon the heat treatment procedure and atmosphere (air, or oxygen). Two mechanisms by which the high-temperature calcination leads to the formation of the disordered phase can be proposed, i.e. oxygen deficiency ($LiNi_{0.5}Mn_{1.5}O_{4-\delta}$) or nickel deficiency ($LiNi_{0.5-x}Mn_{1.5+x}O_4$). The latter supposes the formation of a rock salt impurity as also demonstrated by others [43,44]. Since our XRD patterns did not reveal any sign of impurities, we can safely suggest that the heat treatment at 900 °C in air resulted in oxygen deficiencies with the formation of the disordered spinel phase $LiNi_{0.5}Mn_{1.5}O_{4-\delta}$. Fig. 4a reveals that there was no significant voltage polarization (voltage drop) despite the charge and discharge of the cell at the 1C rate, which indicates that zirconia was not responsible for any significant resistance spike, and hence, it would not be a major rate limiting factor.

Fig. 4b displays the cycling performance of the 1.0 wt% ZrO_2 modified LNMO. The cell was charged at the C/2 rate and discharged at the 40C rate for over a thousand of cycles. It can be seen from Fig. 4b that the cell's capacity gradually increased within the first 50 cycles, and thereafter, decreased and then stabilized on further cycling. As $LiNi_{0.5}Mn_{1.5}O_4$ is coated with ZrO_2, the particles surface may not be fully exposed during initial cycling which explains why there was a capacity gain as the particles become more active after a few cycles. Nonetheless, the ZrO_2-modified LNMO exhibited excellent electrochemical performance. Its discharge capacity was 110 mA h/g at 40C and slightly decayed with extensive cycling (Fig. 4b). After 1200 cycles, the capacity fade was only 15% under such an ultrahigh discharge rate.

Fig. 5 shows the voltage profile of the cell that was subjected to fast charging at the 6C rate and slower discharging at the C/3 rate. In this case, the cell was fabricated with the 1.0 wt% ZrO_2-coated LNMO. In electric vehicles, battery charge and discharge protocols must be optimized in terms of energy, power and cycle life to meet the requirements for local and long distance electrical drives. The scenario of extreme fast charging (XFC) would require about 10-min convenience charge time and 3-h discharge, which is equivalent to the battery being charged at the 6C rate and discharged at the C/3 rate [45]. In our case, the resulting discharge capacity was 134 $mAh.g^{-1}$ and was quite stable throughout the 300 cycles (Inset Fig. 5).

The rate capability of the pure $LiNi_{0.5}Mn_{1.5}O_4$ and ZrO_2-modified LNMO samples are compared in Fig. 6. The pure LNMO had an initial discharge capacity of 125 $mAh.g^{-1}$ up to the 5C rate, whereas, the ZrO_2-modified LNMO exhibited slightly higher initial capacity up to the 10C rate. At the 20C rate and onward, the ZrO_2-modified samples had much better capacity retention compared to the ZrO_2-free sample (Fig. 6). Of note, the sample with 1.0 wt% ZrO_2 exhibited a discharged capacity of 95 $mAh.g^{-1}$, much above all sample, yet at the 80C rate.

The results in Fig. 6 imply that at higher C-rates, the cell's performance may either be limited by the Li-ion diffusivity in the electrolyte solution or charge transfer resistance at the electrode/electrolyte interface, rather than by the Li-ion diffusion within the active particle. We, therefore, estimated the diffusion characteristics time t_s for more evidence.

The characteristic time t_S for the Li-ion to diffuse throughout one electrode to another via an electrolyte solution and with a diffusion length L_S is given by the following equation:

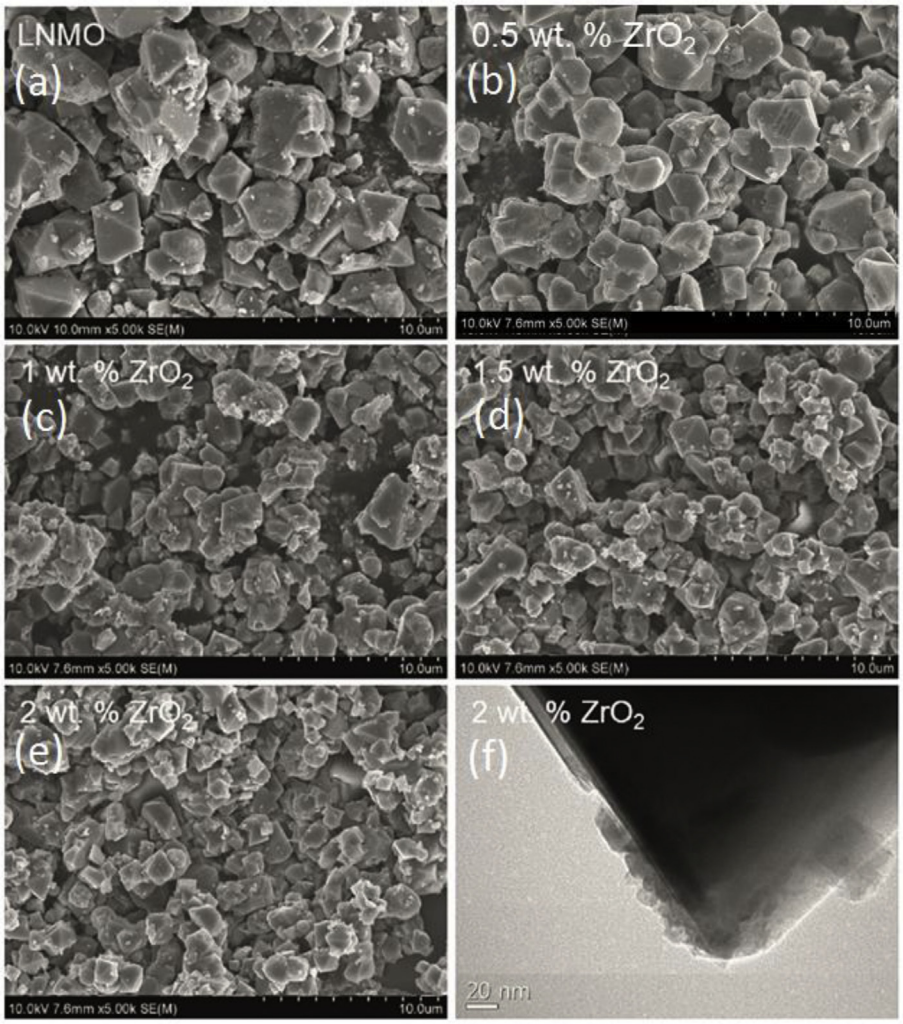

Fig. 2. SEM images of (a) uncoated $LiNi_{0.5}Mn_{1.5}O_4$, (b) 0.5 wt% ZrO_2, (c) 1.0 wt% ZrO_2, (d) 1.5 wt% ZrO_2, (e) 2.0 wt% ZrO_2, coated LNMO and (f) TEM image of 2.0 wt% ZrO_2 coated LNMO.

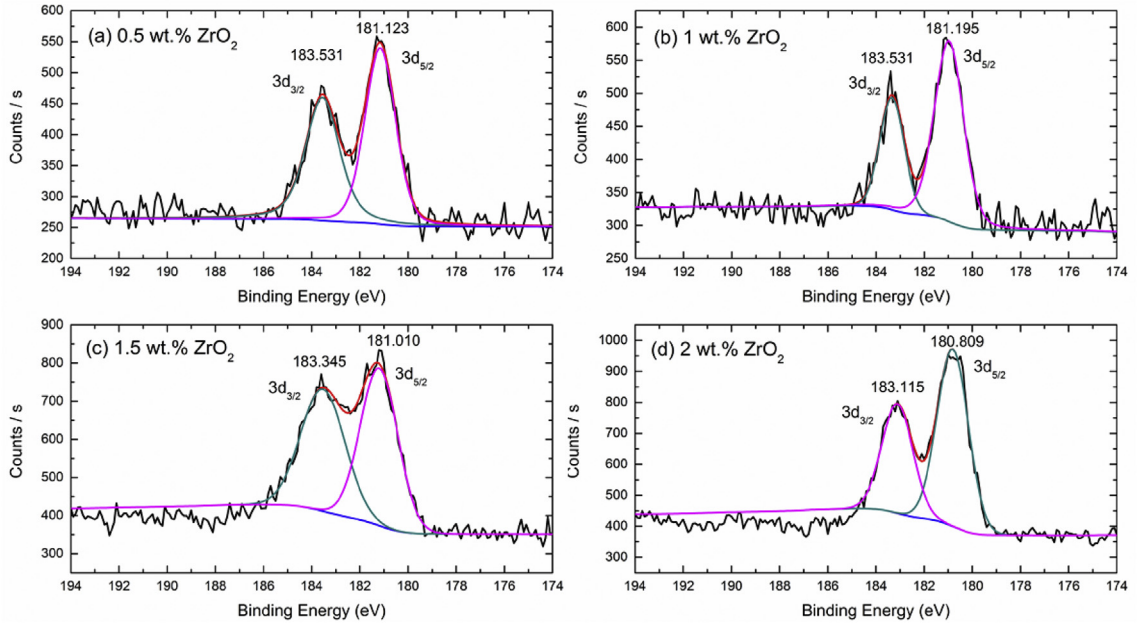

Fig. 3. XPS spectra of $LiNi_{0.5}Mn_{1.5}O_4$ with (a) 0.5 wt% ZrO_2, (b) 1.0 wt% ZrO_2, (c) 1.5 wt% ZrO_2 and (d) 2.0 wt% ZrO_2.

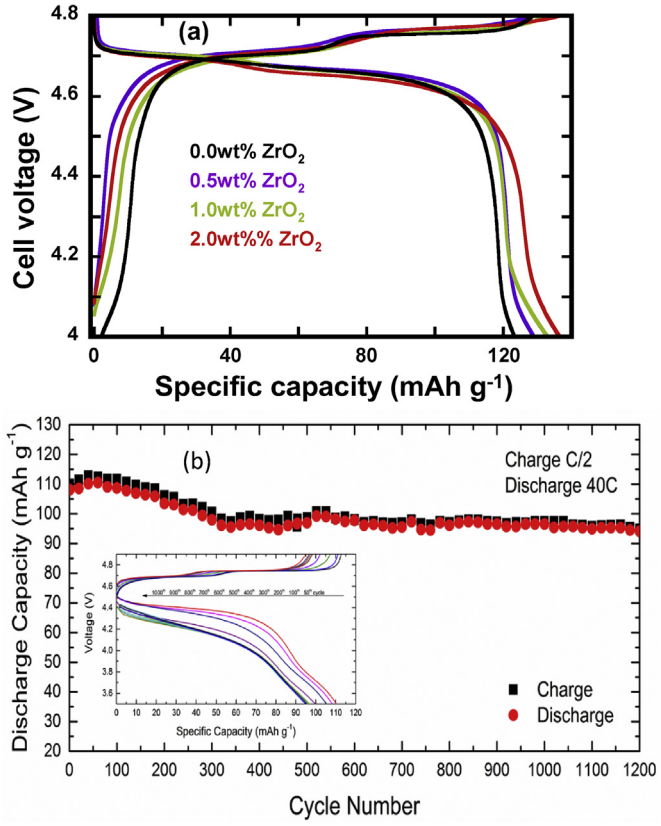

Fig. 4. (a) Charge-discharge profile of $LiNi_{0.5}Mn_{1.5}O_4$ and ZrO_2-modified LNMO after 100 cycles at the 1C rate, and (b) Cycling performance of 1.0 wt% ZrO_2-modified LNMO at C/2 charge and 40C discharge, at room temperature.

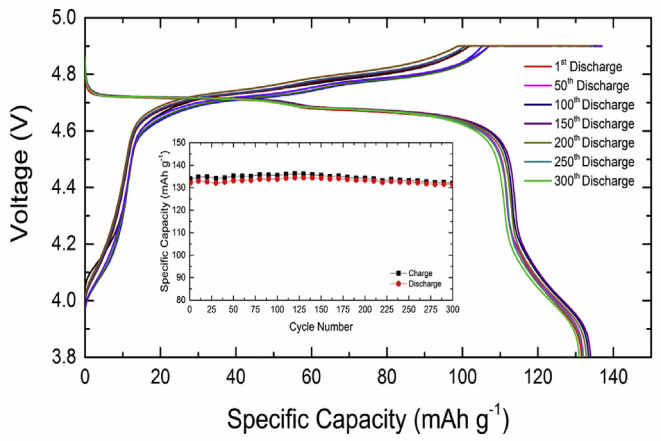

Fig. 5. Voltage profile of a cell made of 1.0 wt% ZrO_2-modified LNMO electrode material. and charged at the 6C rate and discharged at the C/3 rate.

$$t_S = \frac{L_s^2}{D_S} = \frac{(65\,x10^{-4})^2}{5\,x10^{-7}} = 84.5s$$

where D_S is the ionic diffusivity of the electrolyte solution (5×10^{-7} cm^2/s) and *Ls* is the diffusion length (65 μm, including electrode and separator thicknesses) [46].

The characteristic diffusion time t_S within the $LiNi_{0.5}Mn_{1.5}O_4$ solid particle in the electrode is given by:

$$t_S = \frac{L_s^2}{D_S} = \frac{(2\,x10^{-4})^2}{10^{-9}} = 45s$$

The diffusivity value "D_S" was determined experimentally for

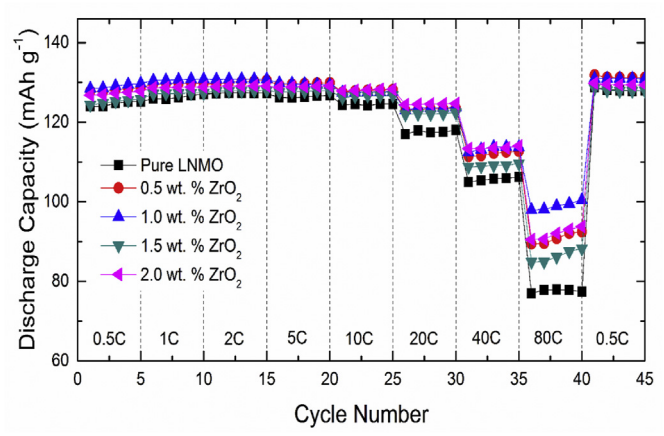

Fig. 6. Discharge capacity of bare- and ZrO_2-modified LNMO (0.5–2.0 wt% ZrO_2). as a function of cycle number at increasing C-rates.

$LiNi_{0.5}Mn_{1.5}O_4$ in our reference [41], and the diffusion length "Ls" value was assumed 2 μm which is in the same range or roughly higher than the particle sizes observed in Fig. 2. From the t_s values, it appears that the solid-state diffusion is not the rate limiting factor up to the 80C discharge rate (80C is equivalent to t_s = 45s), whereas, the ionic diffusion in the electrolyte can be the rate limiting factor starting from the 40C discharge rate (40C is equivalent to t_s = 90s). At higher C-rates beyond 40C, it is unlikely that the interfacial resistance can play a sensible role in being a rate limiting factor. This hypothesis will be discussed later in the below part.

Fig. 7 shows the high-temperature (55°*C*) and high-rate (40C) cycling behavior of the bare- and ZrO_2- modified $LiNi_{0.5}Mn_{1.5}O_4$ samples. The uncoated material had a rapid capacity fading compared to the ZrO_2-modified LNMO during the first 120 cycles (Fig. 7). LNMO retained around 25% of its initial discharge capacity while the presence of ZrO_2 resulted in a much better cycle life with capacity retentions in the range or above 100 mAh.g^{-1} after 120 cycles at 55 °C. We hypothesize that with more ZrO_2, the $LiNi_{0.5}Mn_{1.5}O_4$ particles are protected against direct contact with electrolytes which helped in lessening electrolyte oxidation and thus in improving the cycling performance of the materials. Another observation is that the ZrO_2-free samples exhibited higher cell polarization voltages in comparison with the ZrO_2-modified ones during cycling under the 40C-rate condition (Fig. 7b and c). This may primarily stem from the increase in interfacial resistance due to the formation of a thicker cathode electrolyte interphase (CEI) in the unprotected LNMO. Another reason could the sluggish ionic/electronic transport since the bare LNMO had larger particle sizes compared to the ZrO_2-modified sample (cf. Fig. 2). Fig. S-1 (a-b) shows the discharge curves for 0.5 wt% ZrO_2 LNMO and 2.0 wt% ZrO_2 coated LNMO after 1, 50 and 100 cycles.

The GITT plots, obtained during the step-by-step delithiation/lithiation of the 1.0 wt% ZrO_2-modified $LiNi_{0.5}Mn_{1.5}O_4$, are displayed in Supplementary Figs. S–2. Similar charge-discharge patterns were observed for the other ZrO_2-containing compositions. In every step, the cells were subjected to the C/10 current rate for 1 h, followed by a rest for 3 h to achieve the steady state at the open circuit cell voltages. During this galvanostatic titration, a lithium concentration gradient is developed across the $LiNi_{0.5}Mn_{1.5}O_4$ particles. As a result, cell voltage polarization and depolarization occur during the application and interruption of current, respectively. Fig. 8a and b show selected EIS spectra recorded at 50% state of charge for the 0-2 wt% ZrO_2 modified LNMO. The impedance spectra for the other states of charge are given in the Supplementary Figs. S–3. The cells were held at the open-circuit voltages for 3 h with a voltage decay rate less than 1 mV/h at the end of the rest interval. Under these OCV conditions, the material's voltage lies between oxidation and reduction states where small bias potentials

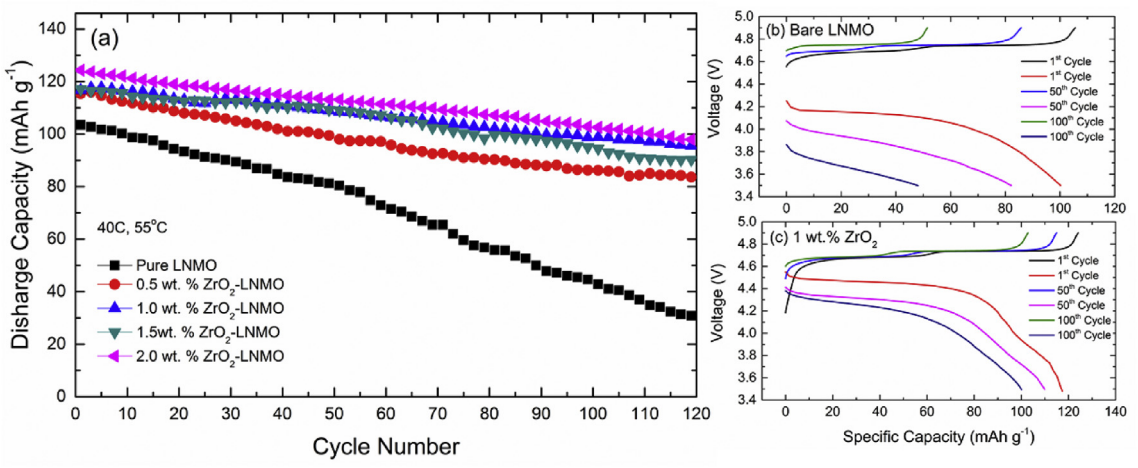

Fig. 7. (a) Cycling performance of LNMO with and without ZrO_2 (0.5–2.0 wt%) at 55 °C, (b) Discharge curves for LNMO, and (c) discharge curves for 1.0 wt% ZrO_2 coated LNMO after 1, 50 and 100 cycles.

during the EIS measurements can induce slight lithiation and delithiation.

The Nyquist plots of LNMO consists of the following main features: 1) a high-frequency intercept due to the ionic resistance of the electrolyte solution along with a minor contribution of the solid electrolyte interphase (SEI), 2) a first semi-circle in the high frequencies due to the electrical conductivity of the coating barrier, 3) a second semi-circle at the medium-high frequencies which is a priori due to the charge transfer resistance at the metallic lithium/electrolyte interface along with the electronic conductivity of active particles, 4) a third semi-circle at the medium-low frequencies which is a priori due to the charge transfer reaction at the electrode/electrolyte interface, and 5) a Warburg response at the lower frequencies part of the plots. The equivalent circuit models (ECM) used to fit the EIS data of the bare and ZrO_2-modified LNMO comprise seven and nine circuit elements, respectively (Fig. S-4a and S-4b). Details on theses ECMs can be found in our previous report [42].

Note that the ZrO_2-free $LiNi_{0.5}Mn_{1.5}O_4$ does not present the high frequency semicircle due to the absence of the coating layer unlike the ZrO_2-modified LNMO. As expected, the ohmic resistance (R1)

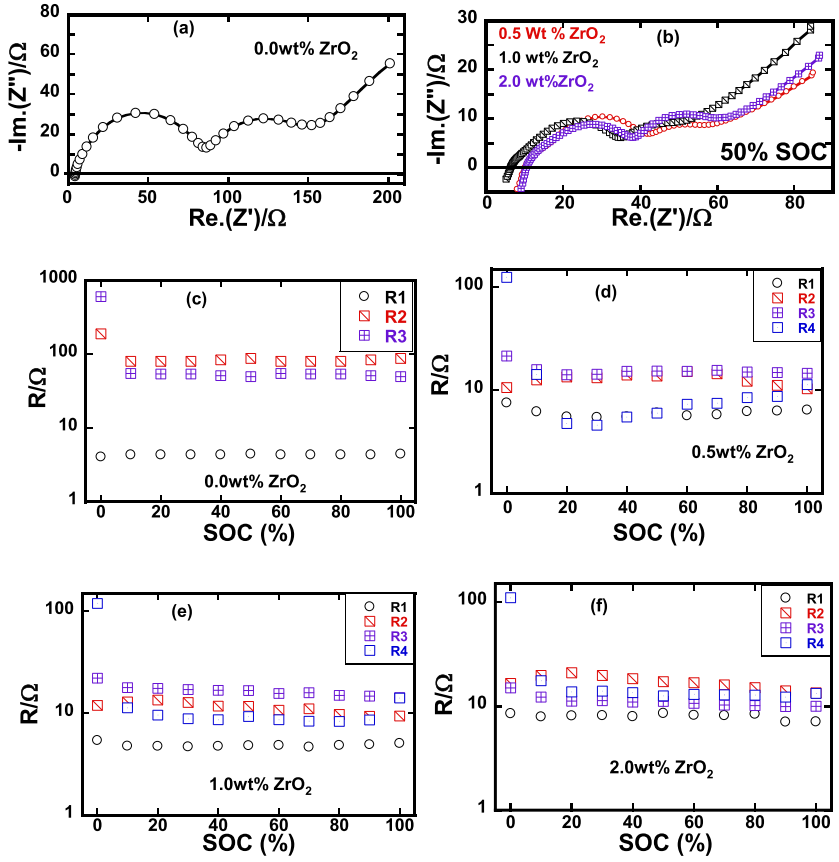

Fig. 8. EIS spectra of (a) bare LNMO, (b) ZrO_2-modified LNMO samples, and calculated resistances as function of SOC for (c) uncoated $LiNi_{0.5}Mn_{1.5}O_4$, (d) 0.5 wt% ZrO_2, (e) 1 wt% ZrO_2, and (f) 2 wt% ZrO_2 coated LNMO.

associated with the electrolyte had quite constant values regardless of states of charge or discharge (Fig. 8c and f). The three and four resistances extracted from the fitting of the impedance spectra for the bare and ZrO_2-modified LNMO are compared in Fig. 8c and f as a function of the states of charge. The interfacial resistances were much lower for the ZrO_2-coated samples in comparison with the uncoated LNMO owing to the beneficial impact of the surface modification in reducing charge transfer resistances (Fig. 8c and f). Following the behavior of the electrolyte resistance (R1), the resistances (R2, R3, and R4) associated with the other processes did not vary significantly except at the beginning of charge. Similar behaviors were observed during discharge as presented in the Supplementary Figs. S–5.

The materials exhibited lower interfacial resistances which did not vary much with the states of charge regardless of the thickness of the ZrO_2 coating (Fig. 8c and f). However, one can observe that the coating resistance R2 was slightly higher for the 2.0 wt% ZrO_2-modified LNMO, which is indicative of the formation of thicker layer on this sample compared to the 0.5–1.5 wt% coated samples. In any cases, the uncoated LNMO had much higher resistances than those of the coated samples, and this could be the reason behind the large cell voltage polarization observed at the higher C-rates (Cf. Fig. 7b and c). The charge transfer resistance at the lithium/electrolyte interface is slightly higher than that of the LNMO/electrolyte interface. The resistance to the electronic conductivity of the active materials LNMO can sum up with the charge transfer resistance at the lithium/electrolyte interface. Nonetheless, the small cell voltage polarization loss, observed during electrochemical measurements, appears to be related to the combined effect of series of resistances rather than to one major contribution of a single process.

4. Conclusion

$LiNi_{0.5}Mn_{1.5}O_4$ particles were coated with different amount of ZrO_2 (0.5–2.0 wt%) using a scalable ball milling process. The phase purity, elemental compositions and microstructure were characterized by XRD, XPS, SEM and TEM. The coating thickness was optimized with respect to the electrochemical performance of $LiNi_{0.5}Mn_{1.5}O_4$. The charge transfer resistance at the $LiNi_{0.5}Mn_{1.5}O_4$/electrolyte interface did not significantly change with the coating amount, indicating that the ZrO_2 surface modification does not impede the rate capability of $LiNi_{0.5}Mn_{1.5}O_4$. The materials with 1.0 and 2.0 wt% ZrO_2 exhibited better cycle life and rate capability at 25 °C. The zirconia-modified materials could withstand current densities up to 80C-rate. The material with 1.0 wt% ZrO_2 ended 1200-cycles at the 40C discharge rate with a capacity of 94 $mAh.g^{-1}$ that is 85.6% capacity retention at 25 °C. However, the material with 2.0 wt% ZrO_2 had much better electrochemical cycling stability at 55 °C (76% capacity retention) compared to the uncoated material. The cells were also cycled according to the recently introduced battery fast charging protocol for electric vehicles (6C-rate charge and C/3-rate discharge). Under these conditions, the retained capacity of the ZrO_2-coated material was 133 $mAh.g^{-1}$ after 300 cycles at room temperature. The origin of the ultrahigh rate capability could be correlated with the extreme high kinetics at the coated interfaces. Moreover, the interfacial charge transfer resistance (R_{ct}) was much lower and did not significantly change with the coating thickness in the case of the surface modified $LiNi_{0.5}Mn_{1.5}O_4$. The electrochemical performances of the ZrO_2-coated $LiNi_{0.5}Mn_{1.5}O_4$ are partially limited by the interfacial resistance at the beginning of charge and electrolyte diffusivity at higher C-rates. The overall results demonstrate that the ZrO_2-surface modification strategy applied to $LiNi_{0.5}Mn_{1.5}O_4$ was very effective in significantly improving the material's rate capability and cycle life performances, a step towards the materialization of extremely fast charged electric vehicles.

Acknowledgment

This research is sponsored by the Laboratory Directed Research and Development Program of Oak Ridge National Laboratory, managed by UT-Battelle, LLC, under Contract No. DE-AC05-00OR22725 for the U.S. Department of Energy.

Appendix A. Supplementary data

Supplementary data related to this article can be found at http://dx.doi.org/10.1016/j.jpowsour.2018.06.065.

References

[1] M.R. Palacín, Recent advances in rechargeable battery materials: a chemist's perspective, Chem. Soc. Rev. 38 (2009) 2565–2575, http://dx.doi.org/10.1039/b820555h.
[2] J.M. Tarascon, M. Armand, Issues and challenges facing rechargeable lithium batteries, Nature 414 (2001) 359–367, http://dx.doi.org/10.1038/35104644.
[3] F. Cheng, J. Liang, Z. Tao, J. Chen, Functional materials for rechargeable batteries, Adv. Mater. 23 (2011) 1695–1715, http://dx.doi.org/10.1002/adma.201003587.
[4] A. Kraytsberg, Y. Ein-Eli, A. Kraytsberg, Y. Ein-Eli, Higher, stronger, better. a review of 5 volt cathode materials for advanced lithium-ion batteries, Adv. Energy Mater 2 (2012) 922–939, http://dx.doi.org/10.1002/aenm.201200068.
[5] D.-W. Jun, C.S. Yoon, U.-H. Kim, Y.-K. Sun, High-energy density core–shell structured Li[Ni $_{0.95}$ Co $_{0.025}$ Mn $_{0.025}$]O $_2$ cathode for lithium-ion batteries, Chem. Mater. 29 (2017) 5048–5052, http://dx.doi.org/10.1021/acs.chemmater.7b01425.
[6] J.-M. Tarascon, Key challenges in future Li-battery research, Philos. Trans. A. Math. Phys. Eng. Sci. 368 (2010) 3227–3241, http://dx.doi.org/10.1098/rsta.2010.0112.
[7] M. Armand, J.-M. Tarascon, Building better batteries, Nature 451 (2008) 652–657, http://dx.doi.org/10.1038/451652a.
[8] L. Guoqiang, LiNi0.5Mn1.5O4 Spinel and its Derivatives as Cathodes for Li-ion Batteries, vol. 4 (n.d.). doi:10.5772/25968.
[9] G.Q. Liu, L. Wen, Y.M. Liu, Spinel LiNi0.5Mn1.5O4 and its derivatives as cathodes for high-voltage Li-ion batteries, J. Solid State Electrochem. 14 (2010) 2191–2202, http://dx.doi.org/10.1007/s10008-010-1061-5.
[10] R. Santhanam, B. Rambabu, Research progress in high voltage spinel LiNi0.5Mn1.5O4 material, J. Power Sources 195 (2010) 5442–5451, http://dx.doi.org/10.1016/j.jpowsour.2010.03.067.
[11] T.-F. Yi, Y. Xie, M.-F. Ye, L.-J. Jiang, R.-S. Zhu, Y.-R. Zhu, Recent developments in the doping of LiNi0.5Mn1.5O4 cathode material for 5 V lithium-ion batteries, Ionics 17 (2011) 383–389, http://dx.doi.org/10.1007/s11581-011-0550-6.
[12] T.-F. Yi, Y.-R. Zhu, X.-D. Zhu, J. Shu, C.-B. Yue, A.-N. Zhou, A review of recent developments in the surface modification of LiMn2O4 as cathode material of power lithium-ion battery, Ionics 15 (2009) 779–784, http://dx.doi.org/10.1007/s11581-009-0373-x.
[13] T.F. Yi, J. Mei, Y.R. Zhu, Key strategies for enhancing the cycling stability and rate capacity of LiNi0.5Mn1.5O4as high-voltage cathode materials for high power lithium-ion batteries, J. Power Sources 316 (2016) 85–105, http://dx.doi.org/10.1016/j.jpowsour.2016.03.070.
[14] M. Hu, X. Pang, Z. Zhou, Review Recent progress in high-voltage lithium ion batteries, J. Power Sources 237 (2013) 229–242, http://dx.doi.org/10.1016/j.jpowsour.2013.03.024.
[15] M. Aklalouch, J.M. Amarilla, R.M. Rojas, I. Saadoune, J.M. Rojo, Sub-micrometric LiCr0.2Ni0.4Mn1.4O4 spinel as 5V-cathode material exhibiting huge rate capability at 25 and 55°C, Electrochem. Commun. 12 (2010) 548–552, http://dx.doi.org/10.1016/j.elecom.2010.01.040.
[16] M. Aklalouch, J.M. Amarilla, I. Saadoune, J.M. Rojo, LiCr0.2Ni0.4Mn1.4O4 spinels exhibiting huge rate capability at 25 and 55°C: analysis of the effect of the particle size, J. Power Sources 196 (2011) 10222–10227, http://dx.doi.org/10.1016/j.jpowsour.2011.08.069.
[17] E.-S. Lee, A. Manthiram, Influence of doping on the cation ordering and charge–discharge behavior of LiMn1.5Ni0.5 − xMxO4 (M = Cr, Fe, Co, and Ga) spinels between 5.0 and 2.0 V, J. Mater. Chem. 1 (2013) 3118, http://dx.doi.org/10.1039/c2ta01171a.
[18] J. Liu, A. Manthiram, Understanding the improved electrochemical performances of Fe-Substituted 5 V spinel cathode LiMn 1.5 Ni 0.5 O 4, J. Phys. Chem. C 113 (2009) 15073–15079, http://dx.doi.org/10.1021/jp904276t.
[19] D.W. Shin, A. Manthiram, Surface-segregated, high-voltage spinel LiMn1.5Ni0.42Ga0.08O4 cathodes with superior high-temperature cyclability for lithium-ion batteries, Electrochem. Commun. 13 (2011) 1213–1216, http://dx.doi.org/10.1016/j.elecom.2011.08.041.
[20] T.-F. Yi, Y. Xie, Y.-R. Zhu, R.-S. Zhu, M.-F. Ye, High rate micron-sized niobium-doped LiMn1.5Ni0.5O4 as ultra high power positive-electrode material for lithium-ion batteries, J. Power Sources 211 (2012) 59–65, http://dx.doi.org/10.1016/j.jpowsour.2012.03.095.
[21] H.-W. Lee, P. Muralidharan, C.M. Mari, R. Ruffo, D.K. Kim, Facile synthesis and electrochemical performance of ordered LiNi0.5Mn1.5O4 nanorods as a high power positive electrode for rechargeable Li-ion batteries, J. Power Sources 196 (2011) 10712–10716, http://dx.doi.org/10.1016/j.jpowsour.2011.09.002.
[22] K.R. Chemelewski, D.W. Shin, W. Li, A. Manthiram, Octahedral and truncated high-

voltage spinel cathodes: the role of morphology and surface planes in electrochemical properties, J. Mater. Chem. 1 (2013) 3347, http://dx.doi.org/10.1039/c3ta00682d.
[23] J.-S. Kim, K. Kim, W. Cho, W.H. Shin, R. Kanno, J.W. Choi, A truncated manganese spinel cathode for excellent power and lifetime in lithium-ion batteries, Nano Lett. 12 (2012) 6358–6365, http://dx.doi.org/10.1021/nl303619s.
[24] X. Zhang, F. Cheng, J. Yang, J. Chen, LiNi0.5Mn1.5O4 Porous Nanorods as High-rate and Long-life Cathodes for Li-ion Batteries, (2013), pp. 2–5, http://dx.doi.org/10.1021/nl401072x.
[25] X. Feng, C. Shen, X. Fang, C. Chen, Nonstoichiometric Li1 ± x Ni0.5Mn1.5O4 with different structures and electrochemical properties, Chin. Sci. Bull. 57 (2012) 4176–4180, http://dx.doi.org/10.1007/s11434-012-5248-2.
[26] J. Zheng, J. Xiao, X. Yu, L. Kovarik, M. Gu, F. Omenya, X. Chen, X.-Q. Yang, J. Liu, G.L. Graff, M.S. Whittingham, J.-G. Zhang, Enhanced Li + ion transport in LiNi0.5Mn1.5O4 through control of site disorder, Phys. Chem. Chem. Phys. 14 (2012) 13515–13521, http://dx.doi.org/10.1039/c2cp43007j.
[27] Y. Fan, J. Wang, Z. Tang, W. He, J. Zhang, Effects of the nanostructured SiO2 coating on the performance of LiNi0.5Mn1.5O4 cathode materials for high-voltage Li-ion batteries, Electrochim. Acta 52 (2007) 3870–3875, http://dx.doi.org/10.1016/j.electacta.2006.10.063.
[28] J. Li, Y. Zhang, J. Li, L. Wang, X. He, J. Gao, AlF3 coating of LiNi0.5Mn1.5O4 for high-performance Li-ion batteries, Ionics 17 (2011) 671–675, http://dx.doi.org/10.1007/s11581-011-0617-4.
[29] J. Liu, A. Manthiram, Understanding the improvement in the electrochemical properties of surface modified 5 V LiMn 1.42 Ni 0.42 Co 0.16 O 4 spinel cathodes in lithium-ion cells, Chem. Mater. 21 (2009) 1695–1707, http://dx.doi.org/10.1021/cm9000043.
[30] H.M. Wu, I. Belharouak, A. Abouimrane, Y.K. Sun, K. Amine, Surface modification of LiNi0.5Mn1.5O4 by ZrP2O7 and ZrO2 for lithium-ion batteries, J. Power Sources 195 (2010) 2909–2913, http://dx.doi.org/10.1016/j.jpowsour.2009.11.029.
[31] J.W. Kim, D.H. Kim, D.Y. Oh, H. Lee, J.H. Kim, J.H. Lee, Y.S. Jung, Surface chemistry of LiNi0.5Mn1.5O4particles coated by Al2O3using atomic layer deposition for lithium-ion batteries, J. Power Sources 274 (2015) 1254–1262, http://dx.doi.org/10.1016/j.jpowsour.2014.10.207.
[32] Z. Chen, Y. Qin, K. Amine, Role of surface coating on cathode materials for lithium-ion batteries, J. Mater. Chem. 20 (2010) 7606–7612, http://dx.doi.org/10.1039/c0jm00154f.
[33] H. Liu, C. Cheng, K. Zhang, The effect of ZnO coating on LiMn2O4 cycle life in high temperature for lithium secondary batteries, Mater. Chem. Phys. 101 (2007) 276–279, http://dx.doi.org/10.1016/j.matchemphys.2006.05.006.
[34] J.-H. Shim, S. Lee, S.S. Park, Effects of {MgO} {coating} on the {structural} and {electrochemical} {characteristics} of {LiCoO}2 as {cathode} {materials} for {lithium} {ion} {battery}, Chem. Mater. 26 (2014) 2537–2543, http://dx.doi.org/10.1021/cm403846a.
[35] X. Li, K. Zhang, M. Wang, Y. Liu, M. Qu, W. Zhao, J. Zheng, Dual functions of zirconium modification on improving the electrochemical performance of Ni-rich LiNi $_{0.8}$ Co $_{0.1}$ Mn $_{0.1}$ O $_{2}$, Sustain, Energy Fuel. (2018) 413–421, http://dx.doi.org/10.1039/C7SE00513J.
[36] X. Li, K. Zhang, D. Mitlin, Z. Yang, M. Wang, Y. Tang, F. Jiang, Y. Du, J. Zheng, Fundamental insight into Zr modification of Li- and Mn-Rich cathodes: combined transmission electron microscopy and electrochemical impedance spectroscopy study, Chem. Mater. (2018), http://dx.doi.org/10.1021/acs.chemmater.7b04861 acs.chemmater.7b04861.
[37] S. Amaresh, K. Karthikeyan, K.J. Kim, M.C. Kim, K.Y. Chung, B.W. Cho, Y.S. Lee, Facile synthesis of ZrO2 coated Li2CoPO4F cathode materials for lithium secondary batteries with improved electrochemical properties, J. Power Sources 244 (2013) 395–402, http://dx.doi.org/10.1016/j.jpowsour.2012.12.010.
[38] S. Lim, J. Cho, PVP-functionalized nanometre scale metal oxide coatings for cathode materials: successful application to LiMn2O4 spinel nanoparticles, Chem. Commun. (2008) 4472–4474, http://dx.doi.org/10.1039/b807973k.
[39] S.T. Myung, K. Izumi, S. Komaba, Y.K. Sun, H. Yashiro, N. Kumagai, Role of alumina coating on Li − Ni − Co − Mn − O particles as positive electrode material for lithium-ion batteries, Chem. Mater. 17 (2005) 3695–3704, http://dx.doi.org/10.1021/CM050566S.
[40] J. Lu, C. Zhan, T. Wu, J. Wen, Y. Lei, A.J. Kropf, H. Wu, D.J. Miller, J.W. Elam, Y.-K. Sun, X. Qiu, K. Amine, Effectively suppressing dissolution of manganese from spinel lithium manganate via a nanoscale surface-doping approach, Nat. Commun. 5 (2014) 5693, http://dx.doi.org/10.1038/ncomms6693.
[41] R. Amin, I. Belharouk, Part I: electronic and ionic transport properties of the ordered and disordered LiNi0.5Mn1.5O4spinel cathode, J. Power Sources 348 (2017) 311–317, http://dx.doi.org/10.1016/j.jpowsour.2017.02.071.
[42] R. Amin, I. Belharouak, Part-II: exchange current density and ionic diffusivity studies on the ordered and disordered spinel LiNi0.5Mn1.5O4cathode, J. Power Sources 348 (2017) 318–325, http://dx.doi.org/10.1016/j.jpowsour.2017.02.070.
[43] J.C. Arrebola, A. Caballero, M. Cruz, L. Hernán, J. Morales, E.R. Castellón, Crystallinity control of a nanostructured LiNi0.5Mn 1.5O4 spinel via polymer-assisted synthesis: a method for improving its rate capability and performance in 5 V lithium batteries, Adv. Funct. Mater. 16 (2006) 1904–1912, http://dx.doi.org/10.1002/adfm.200500892.
[44] X. Zhang, F. Cheng, K. Zhang, Y. Liang, S. Yang, J. Liang, J. Chen, Facile polymer-assisted synthesis of LiNi0.5Mn1.5O4 with a hierarchical micro–nano structure and high rate capability, RSC Adv. 2 (2012) 5669, http://dx.doi.org/10.1039/c2ra20669b.
[45] T. Inl, Battery test manual for plug-in hybrid electric vehicles, Contract 158 (2010) 1720–1723 INL/EXT-07-12536.
[46] B. Delattre, R. Amin, J. Sander, D. Coninck, A.P. Tomsia, Y. Chiang, Impact of Pore Tortuosity on Electrode Kinetics in Lithium Battery Electrodes ;: Study in Directionally Freeze-Cast 165 (2018), pp. 388–395, http://dx.doi.org/10.1149/2.1321802jes.